JOURNAL OF APPLIED ELECTROCHEMISTRY **28** (1998) 1251–1260

Rotating cylinder Hull cell study of anomalous codeposition of binary iron-group alloys

N. ZECH, E. J. PODLAHA*, D. LANDOLT‡

Laboratoire de Métallurgie Chimique, Département des Matériaux, Ecole Polytechnique Fédérale de Lausanne (EPFL), MX-C Ecublens, Lausanne, Switzerland, CH-1015

Received 12 February 1998; accepted in revised form 12 May 1998

The anomalous codeposition of the iron group metals was investigated using the rotating cylinder Hull (RCH) cell. Single metals and binary alloys of iron, nickel and cobalt were deposited in the RCH cell and the partial current densities were determined as a function of length by position sensitive X-ray fluorescence analysis. The measured overall polarization behaviour was used as a boundary condition for the numerical calculation of the potential distribution along the cylinder using the Laplace equation. By combining the results the partial current density potential curves were established. Experiments performed at different rotation rates confirmed the inhibiting effect of the less noble metal on the deposition of the more noble metal. The inhibiting effect of iron on nickel disappeared when iron reached the limiting current. Strong evidence was found that in binary alloy deposition of iron, cobalt and nickel the reaction rate of the less noble metal is promoted by the presence of the more noble component.

Keywords: *electrodeposition*, *anomalous codeposition*, *iron-group alloys*, *rotating cylinder Hull cell*

1. Introduction

Electrodeposited thin films of binary alloys of the iron group metals Fe, Co and Ni are of interest for different applications in electronics and microtechnology. The best known example is permalloy, an FeNi alloy used in soft magnetic read/write heads [1–3]. The cobalt alloys also present interesting magnetic properties making them candidates for disc storage media [2, 4–6]. Iron-group alloys have been proposed as substitutes for decorative Ni [7–9] and they have found interest for microfabrication by the LIGA process [10, 11].

The electrodeposition behaviour of iron-group alloys belongs to Brenner's anomalous codeposition category [12] which is characterized by an unusually large concentration of the less noble element in the electrodeposit. The behaviour is due to an inhibition effect of the less noble metal on the codepositing more noble metal [13]. The inhibition of nickel by iron during electrodeposition of FeNi is well documented [2, 12, 14–18] and quantitative models have been developed [14, 19, 20]. To avoid depositing an excess of the less noble element, its concentration in the electrolyte is often chosen to be much lower than that of the more noble species. As a consequence, during alloy deposition the reaction rate of the less noble metal may be under mass transport control. This, in turn, can influence the inhibiting action [14, 20].

The aim of this work is to use the rotating cylinder Hull (RCH) cell [21] for the characterization of the electrodeposition behaviour of iron-group binary alloys over a wide range of conditions in both the kinetic and mass transport regimes. The use of an electrode geometry with a uniform current distribution for the determination of the partial current densities by chemical analysis of the deposits requires a large number of deposition experiments (one for each measuring point) and therefore is very time consuming. The RCH cell [21–25], on the other hand, allows one to deposit a metal or alloy over a wide range of current densities in a single experiment, similar to a conventional Hull cell but under controlled hydrodynamic conditions. Due to the particular arrangement of the cathode and the anode a well controlled nonuniform current distribution is developed along the cathode length [21, 24]. At the near end of the cathode the current density is high while at the far end a low current density prevails. After a deposition experiment in the RCH cell one determines the deposit composition and thickness as a function of position along the cathode length. From these measurements, the partial current density of each metal reaction can be determined as a function of potential provided the current density and potential distribution along the cathode length are known. The primary current distribution in the RCH cell was calculated numerically [22] and resembles that of the conventional Hull cell [26, 27]. The secondary current distribution in the RCH cell has been calculated for Butler–Volmer kinetics and was found to compare well with experiments [24]. In systems where the

* Present address: Louisiana State University, Baton Rouge, LA, USA.
‡ Author to whom correspondence should be addressed.

0021-891X

electrode kinetics are not known *a priori*, the cathode boundary condition can be expressed by a measured polarization curve [23]. The calculation of the potential distribution on the RCH cathode allows one to convert the length scale into a potential scale and thus determine partial current density–potential curves from a position sensitive chemical analysis.

In the present study the RCH cell is used for the investigation of anomalous codeposition of iron group metals. The partial current density distribution of the codeposited metals and of hydrogen were obtained from position sensitive X-ray fluorescence analysis of the deposits and the potential distribution was calculated numerically using the polarization curves measured under uniform current distribution as a boundary condition.

2. Experimental details

2.1. *Electrochemical cell*

A rotating cylinder Hull cell (RCH) configuration [22] was used for galvanostatic depositions. The working electrode was a copper cylinder having a diameter of 1.5 cm, the rotation rate was controlled by a Pine Instruments rotator. The cylinder electrodes were recessed 0.25 cm into the insulating shaft. The electrode length was 6 cm. An insulating cylindrical wall with a diameter of 5.4 cm was placed around the electrode in order to induce a controlled nonuniform primary current distribution along the electrode length. Three coiled Pt wires were used as anodes. They were placed in glass tubes which were sealed at the end with a glass frit (5 μm pore size). In this way the anolyte and catholyte were separated avoiding contamination of the catholyte by anodically produced ferric ions. During deposition an average current density of 25 mA cm^{-2} was applied for 600 s. The resulting deposit thickness varied typically from 1 to 15 μm along the cathode height.

Potentiodynamic polarization curves were measured in the same set-up but without the insulating cylindrical wall, thus establishing a uniform current distribution on the cathode. The rotating cylinder electrode length was 1 cm. A saturated mercury sulfate reference electrode (MSE) with a Luggin capillary was employed.

2.2. *Instrumentation*

A potentiostat (Autolab, model PGSTAT20) interfaced to a 486/80 PC was used for both galvanostatic and potentiodynamic experiments. For measuring polarization curves the potential was scanned at 2 mV s^{-1} from the open circuit potential until a current of 100 mA cm^{-2} was reached. The ohmic drop between the reference and working electrode was measured by impedance spectroscopy (Zahner) varying the frequency between 10–110 kHz for an amplitude of 10 mV. The ohmic resistance could readily be measured from the intercept of the imaginary part in a Nyquist plot. All potentials reported in this paper were corrected for ohmic drop.

2.3. *Solutions*

Acid sulfate electrolytes were chosen for this study, containing metal sulfates ($NiSO_4.6\,H_2O$, $CoSO_4.7H_2O$ and/or $FeSO_4.7\,H_2O$), boric acid and sodium sulfate. The compositions of the solutions used are listed in Table 1. The solutions were made up using double distilled water which was sparged with nitrogen for one hour before solution preparation. In all solutions the total amount of sulfate ions was the same. The pH was adjusted to a value of 3 with sulfuric acid. The freshly prepared solutions were sparged before experiments, and a nitrogen flux was maintained above the solution during experiments. The pH was measured before and after every deposition experiment or polarization curve measurement (Jenway pH-meter 3010). In the event of a pH change, the value was corrected by adding sulfuric acid. All experiments were conducted at a temperature of 25 °C. The conductivity of the solutions was determined by two-point-resistance measurement (Tacussel électronique, conductivity meter CD 7 N).

2.4. *Deposit analysis*

A microspot X-ray fluorescence spectrometer (Kevex Instruments) in connection with Omicron software was used for the determination of the composition and thickness of the deposits. Pure metals were used as standards. On every cylinder of 6 cm length the deposit was analyzed at a 30 equidistant points along the cylinder height. The partial current densities of the alloy components were calculated from these XRF measurements using Faraday's law.

2.5. *Procedure for data evaluation*

The procedure used for data evaluation (described in [23]) is schematically shown in Fig. 1. The composition and thickness of alloy deposits produced in the RCH cell were determined as a function of position using XRF. In an independent experiment the overall polarization curve was measured using a conventional rotating cylinder electrode (RCE) of equal radius. The rotation rate in these experiments was the same as during electrodeposition in the RCH cell. The polarization curve was digitized and served as a

Table 1. Electrolyte compositions

Deposit	*$NiSO_4$* /M	*$CoSO_4$* /M	*$FeSO_4$* /M	*H_3BO_3* /M	*Na_2SO_4* /M
FeNi	0.2		0.025	0.4	0.5
FeCo		0.2	0.025	0.4	0.5
CoNi	0.2	0.025		0.4	0.5
Ni	0.2			0.4	0.525
Co		0.2		0.4	0.525
Fe			0.025	0.4	0.7

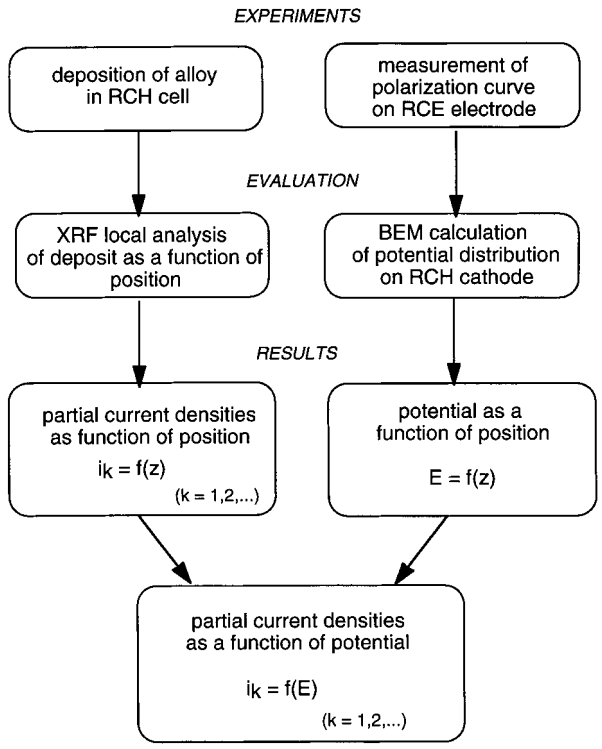

Fig. 1. Procedure for data evaluation with the RCH cell.

boundary condition in Laplace's equation for the numerical calculation of the potential distribution using a program based on the boundary element method (BEM) [28]. The calculation yielded the potential as a function of position on the cathode. By combining this result with that for the measured partial current densities as a function of height the partial current densities of the alloy components were computed as a function of potential. The partial current density of the side reaction (hydrogen) was obtained by subtracting the sum of the partial metal deposition current densities from the total current density. The described procedure yielded a complete set of partial current density–potential curves from a single deposition experiment.

3. Results

Results for codeposition of iron with nickel in the RCH cell are presented in Fig. 2. The weight percentage of iron, Figure 2(a), and the deposit thickness, Figure 2(b), are shown as a function of the calculated potential for three different rotation rates: 300, 800 and 1400 rpm. Figure 2(c) shows the polarization curve for the same systems measured on a RCE. The latter data are required for converting the electrode length scale to the potential scale as described in the experimental section.

In these experiments the ferrous ion concentration in the electrolyte was only 0.025 M to reach mass transport limiting conditions. The nickel concentration, on the other hand, was large (0.2 M) and therefore, changes in rotation rate should only influence the iron deposition rate. The data of Fig. 2(a) show

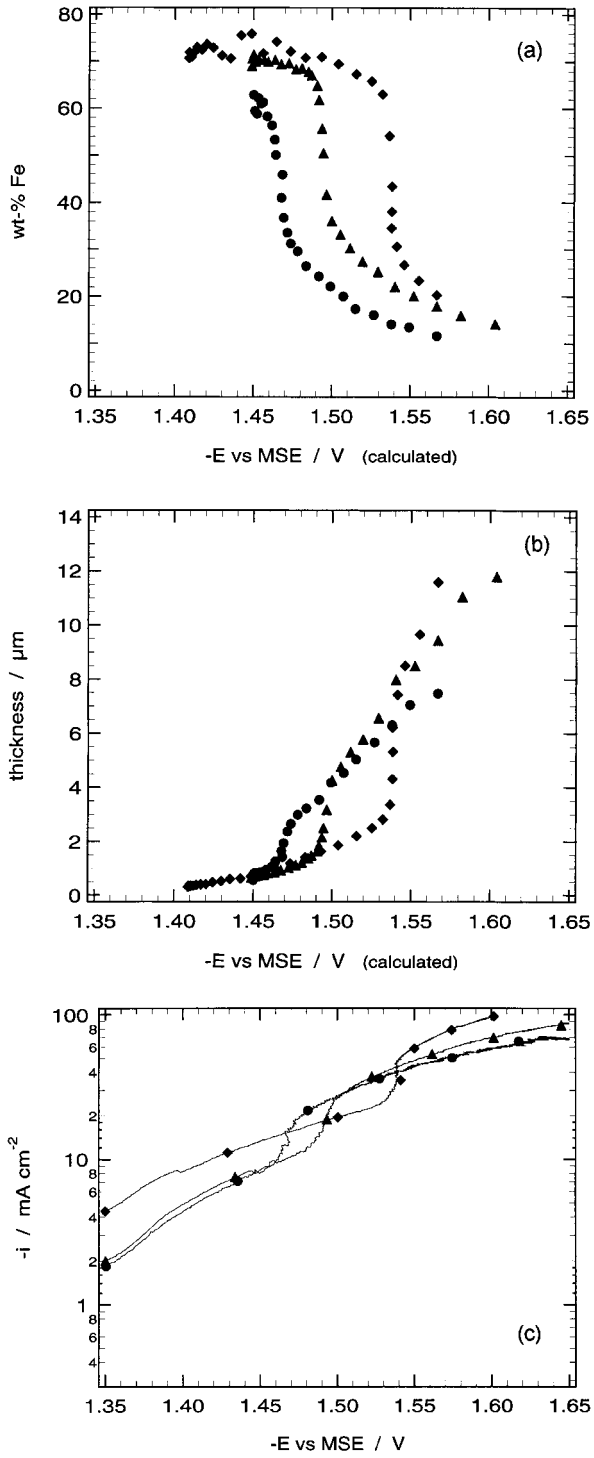

Fig. 2. Concentration in weight percent of Fe in the FeNi alloy (a) and deposit thickness (b) as a function of calculated potential for the codeposition of Fe and Ni in the RCH cell. Also shown are polarization curves (c) measured on the RCE under otherwise identical conditions. Electrolyte concentration: 0.025 M Fe + 0.2 M Ni. Rotation rates: (●) 300, (▲) 800 and (■) 1400 rpm.

that the iron content of the alloy decreases drastically with the potential becoming more negative, the behaviour depending on rotation rate. The deposit thickness also varies along the electrode, it is smallest at less negative potential (low current density region). The partial current densities of nickel, iron and for the side reaction (hydrogen) are shown in Fig. 3(a), (b) and (c), respectively, as a function of the calcu-

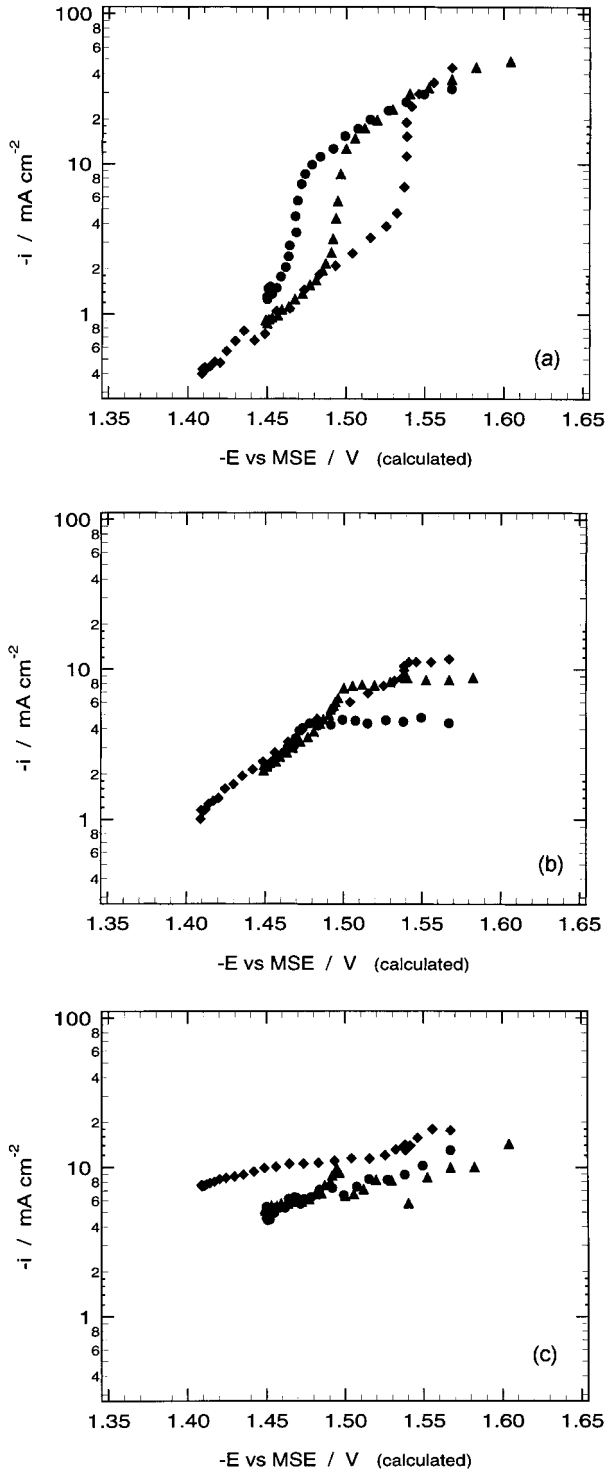

Fig. 3. Partial current densities of Ni (a), Fe (b) and the side reaction (c) for the deposition of FeNi alloy in the RCH cell, calculated from the data of Fig. 2.

lated potential. The partial current of nickel exhibits a characteristic 'jump' at a potential which depends on the applied rotation rate. This jump coincides with iron reaching the limiting current as is shown by the data of Fig. 3(b). At 300 rpm the limiting current for iron deposition is reached near −1.47 V, at 800 rpm near −1.49 V and at 1400 rpm near −1.53 V. A similar effect of the iron mass transport limit on nickel deposition behavior has been observed by Andricacos *et al.* [17] who studied FeNi codeposition on a rotating disc electrode in chloride electrolytes. The behaviour is related to a change in surface coverage of adsorbed iron species as calculated by Matlosz [14] who used kinetic data from Dahms and Croll [1].

The partial current density of the side reaction is shown in Fig. 3(c) for the different rotation rates. The partial current density for 1400 rpm is clearly higher than those for 800 rpm and 300 rpm which are roughly the same. In a solution of pH 3 one would expect the side reaction to be limited by the rate of discharge of protons. This could explain the observed increase of the partial current density at high rotation rate. Since the partial current density for the side reaction was determined from the difference of two measured values (the total current density at the RCE and the partial metal deposition current densities from RCH) the accuracy of these data is limited. This may explain that in Fig. 3(c) the rotation rate dependence is not systematic.

The single metals nickel and iron, respectively, were deposited at 800 rpm. The electrolyte for the Ni metal deposition contained 0.2 M nickel ion and that for iron deposition contained 0.025 M ferrous ion. The measured partial current densities for single metal deposition together with those for FeNi alloy deposition are shown in Fig. 4. The partial current densities for single metal deposition were determined from the measured deposit thickness. The potential scale was calculated numerically as described in the experimental section, using measured polarization curves (not shown) as a boundary condition. The results confirm that nickel deposition is inhibited by the codepositing iron as expected from the literature [17]. On the other hand, the iron partial current density for FeNi alloy deposition is higher than for Fe single metal deposition. This unexpected observation suggests that the codepositing nickel has a catalytic effect on iron deposition.

Using the same conditions as above CoNi alloys were electrodeposited in the RCH cell. The concen-

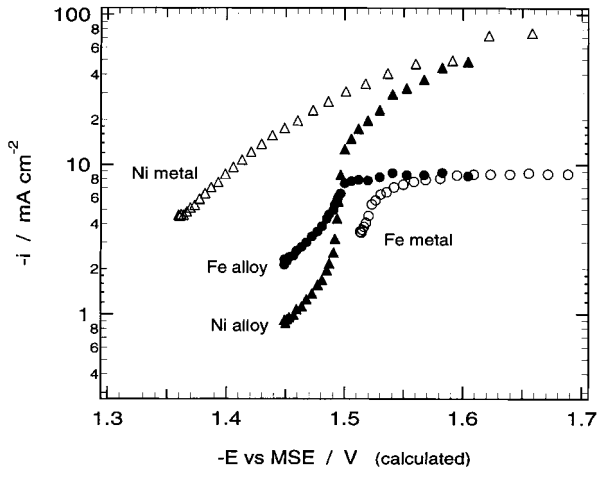

Fig. 4. Partial current densities of Fe and Ni measured during single metal deposition and during codeposition in the RCH cell. Electrolyte concentration for single metal deposition: 0.025 M Fe and 0.2 M Ni, respectively. Electrolyte concentration for alloy deposition: 0.025 M Fe + 0.2 M Ni. Rotation rate: 800 rpm.

tration of cobalt in the solution was 0.025 M and that of nickel was 0.2 M and the rotation rate was 300, 800 and 2100 rpm. Results are given in Fig. 5 showing (a) the weight percentage of cobalt and (b) the deposit thickness. The polarization behaviour determined with the RCE is shown in Fig. 5(c). The data of Fig. 5(a) show that a higher rotation rate leads to a higher concentration of Co in the alloy. This indicates that cobalt deposition under the conditions of the experiment was controlled by mass transport. In agreement with this, the concentration of cobalt in the alloy decreases with increasing current density (overpotential) because the deposition rate of nickel increases with potential but not that of cobalt. The partial current densities measured for the CoNi system are shown in Fig. 6. The nickel partial current is rather insensitive to rotation rate at all potentials

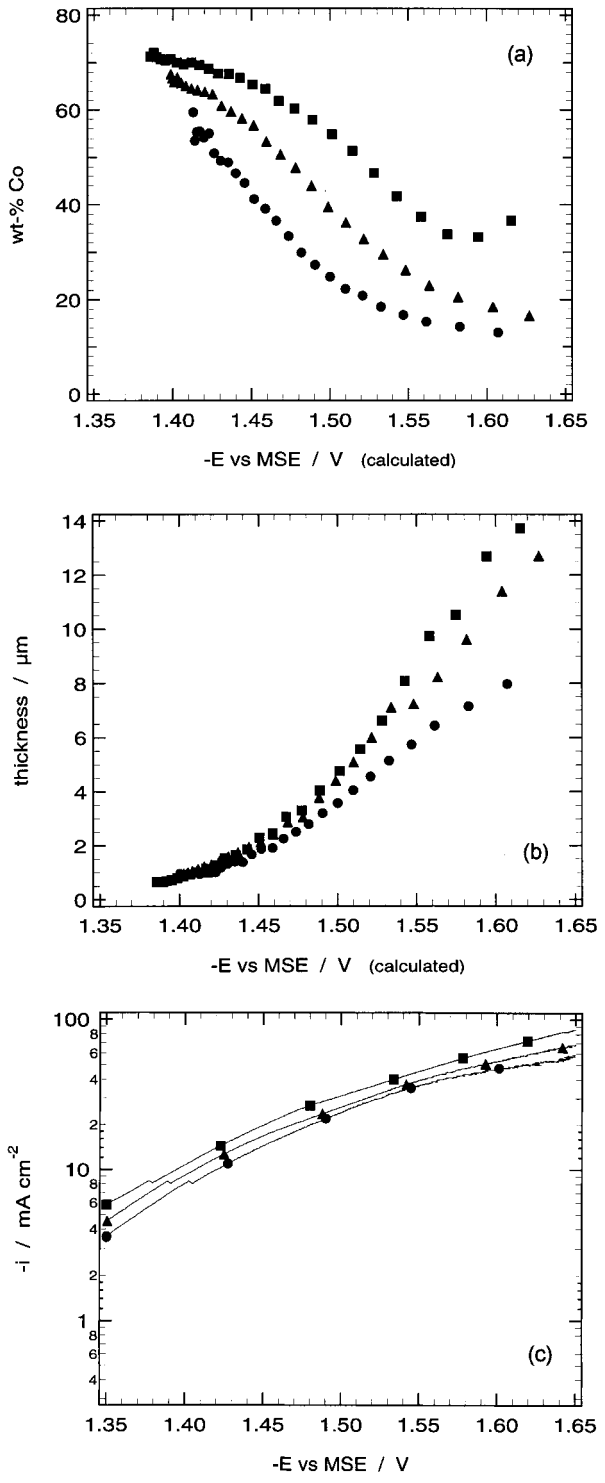

Fig. 5. Concentration in weight percent of Co in the CoNi alloy (a) and deposit thickness (b) as a function of calculated potential for the codeposition of Co and Ni in the RCH cell. Also shown are polarization curves (c) measured on the RCE under otherwise identical conditions. Electrolyte concentration: 0.025 M Co + 0.2 M Ni. Rotation rates: (●) 300, (▲) 800 and (■) 2100 rpm.

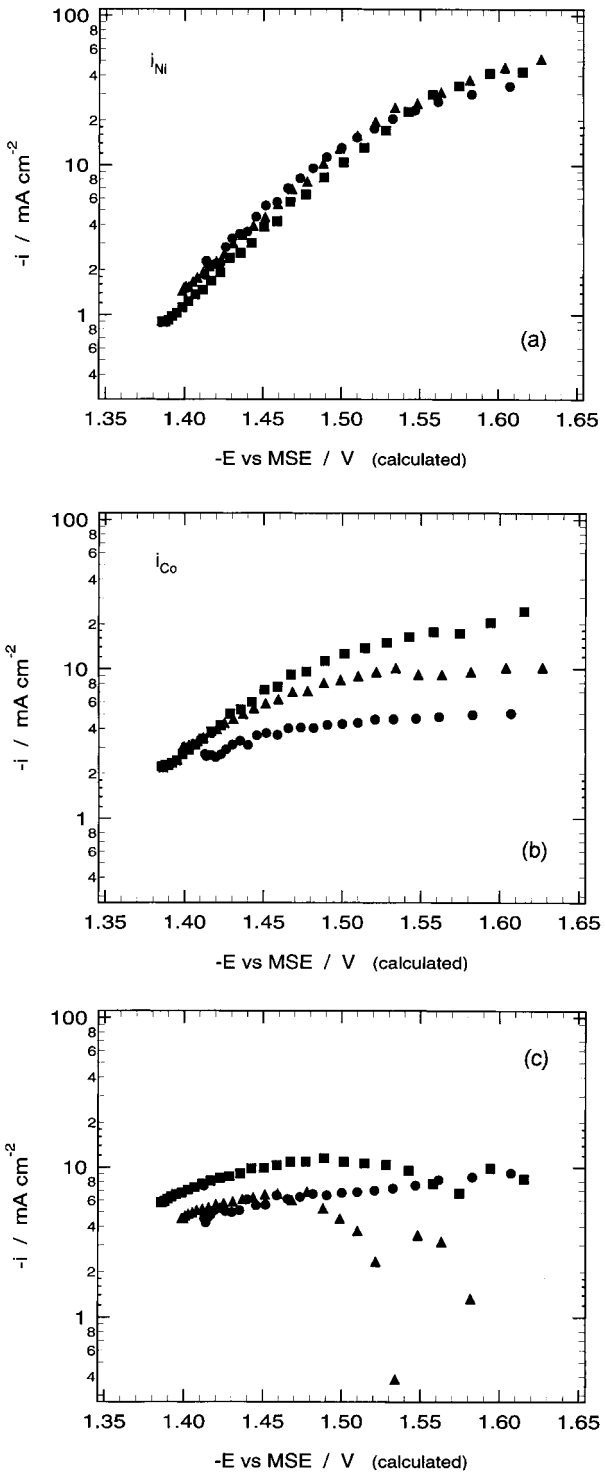

Fig. 6. Partial current densities of Ni (a), Co (b) and the side reaction (c) for the deposition of CoNi alloy in the RCH cell, calculated from the data of Fig. 5.

indicating that it is kinetically controlled (Fig. 6(a)). Cobalt on the other hand, is mass transport limited over a large potential range (Fig. 6(b)). In contrast to the behaviour of the Fe–Ni system no characteristic jump in the nickel partial current occurs when the cobalt limiting current is reached. The side reaction appears to be diffusion limited (Fig. 6(c)) throughout most of the potential range studied.

The codeposition of iron and cobalt was studied using a concentration of ferrous ion of 0.025 M and a cobalt concentration of 0.2 M. The rotation rate was 300, 800 and 2100 rpm, respectively. Results are given in Fig. 7. The iron content of the alloy (Fig. 7(a)) decreases with increasing overvoltage and with decreasing rotation rate. In contrast to FeNi deposition (Fig. 3(a)) no characteristic jump in concentration is observed. The deposit thickness (Fig. 7(b)) increases monotonically towards increasingly negative potentials and it depends only weakly on rotation rate. The polarization curve (Fig. 7(c)) is independent of rotation rate over most of the potential region of interest.

The partial current densities of iron, cobalt and the side reaction calculated from the data of Fig. 7 are shown in Fig. 8. The partial current density of iron varies relatively little with rotation rate and it does not exhibit a well defined limiting current plateau. This is a different behaviour than observed for codeposition of iron with nickel under otherwise identical conditions (Fig. 3(b)). The partial current density for the side reaction (Fig. 8(c)) goes through a maximum. The observed effect of rotation rate and the small dependence on potential suggests that it is largely diffusion limited.

The partial current densities for single metal deposition of iron and cobalt are shown in Fig. 9 and they are compared to the partial current densities for FeCo alloy deposition. The data indicate that cobalt deposition is inhibited by the codepositing iron. The rate of Fe deposition, on the other hand, is increased by the codeposition of cobalt.

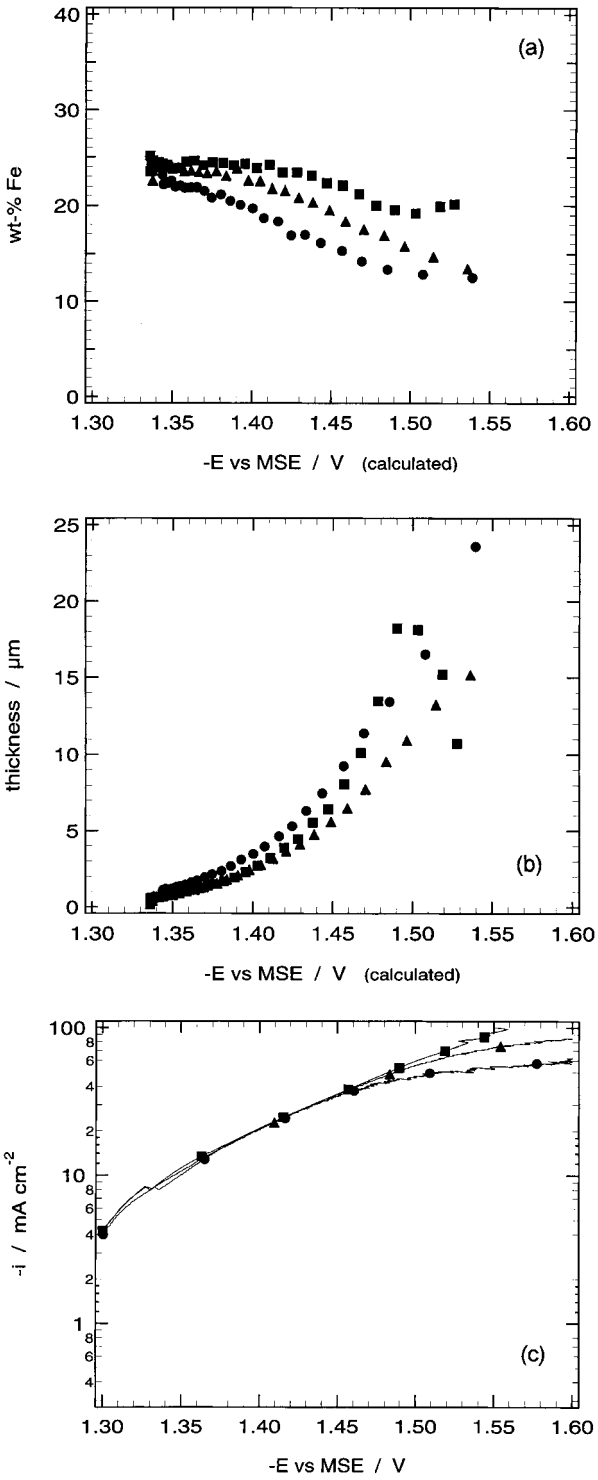

Fig. 7. Concentration in weight percent of Fe in the FeCo alloy (a) and deposit thickness (b) as a function of calculated potential for the codeposition of Fe and Co in the RCH cell. Also shown are polarization curves (c) measured on the RCE under otherwise identical conditions. Electrolyte concentration: 0.025 M Fe + 0.2 M Co. Rotation rates: (●) 300, (▲) 800 and (■) 2100 rpm.

4. Discussion

4.1. *Comparison of RCH cell and RCE results*

The RCH configuration has been used in the present work to examine partial current densities of alloy components and of the side reaction as a function of potential and rotation rate during anomalous codeposition of iron group metals. The use of the RCH cell permits to construct a partial current density–potential curve from a single experiment because of a multitude of analysis points along the cylinder height. On the other hand, the potentials are calculated rather than measured. Before discussing the results for alloy deposition obtained in this study it is therefore necessary to verify that RCH method yields meaningful data.

Previously, it has been shown that approximate potentials can be estimated by simply using an analytical formula for primary current distribution in conjunction with an overall current–potential curve [25]. This approach has, for example, been used by two of the present authors for the study of the effect of different variables on the induced codeposition behaviour of molybdenum with nickel [29]. In the present study a more precise calibration of the potential scale was desired. This is based on a numerical calculation of the secondary current distribution

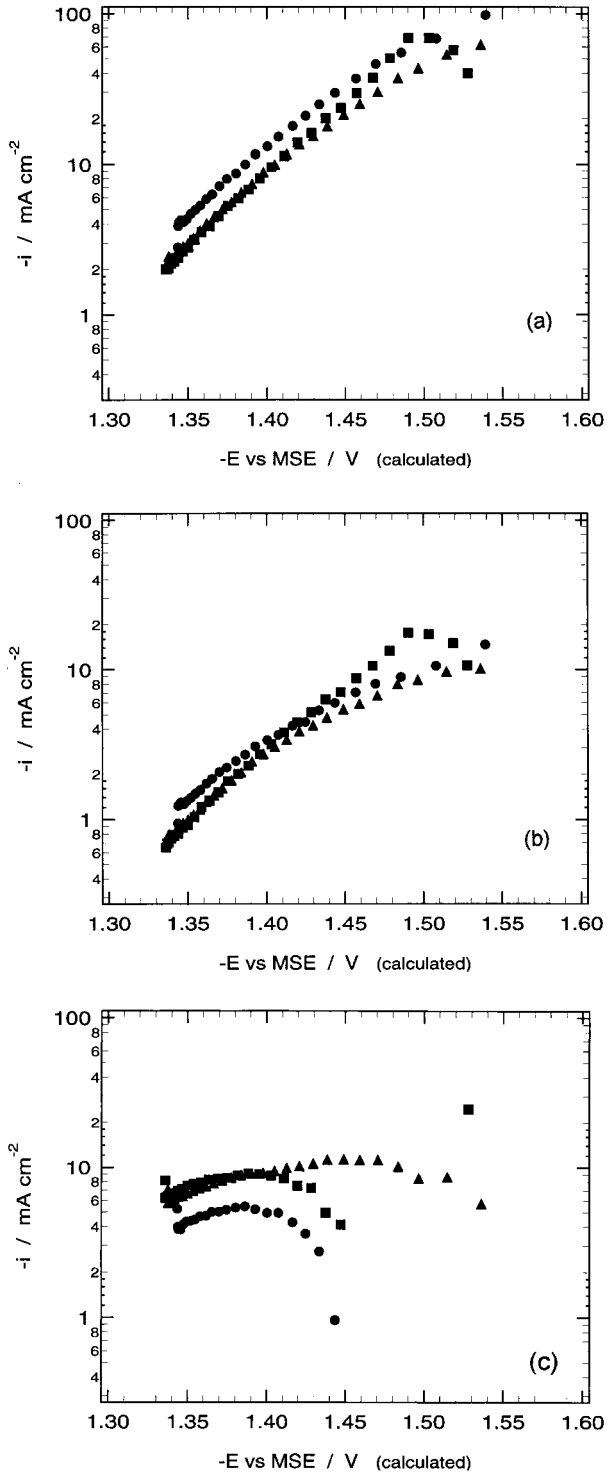

Fig. 8. Partial current densities of Co (a), Fe (b) and the side reaction (c) for the deposition of FeCo alloy in the RCH cell, calculated from the data of Fig. 7.

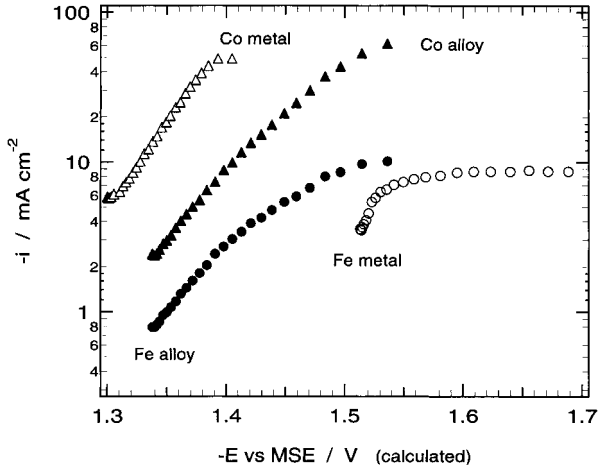

Fig. 9. Partial current densities of Fe and Co measured during single metal deposition and during codeposition in the RCH cell. Electrolyte concentration for single metal deposition: 0.025 M Fe and 0.2 M Co, respectively. Electrolyte concentration for alloy deposition: 0.025 M Fe + 0.2 M Co. Rotation rate: 800 rpm.

using as a boundary condition the measured overall polarization curve, obtained in a separate experiment on a RCE of the same diameter under uniform current distribution conditions. In practice such an experiment can be performed in the same cell by simply removing the insulating cylindrical wall which determines the RCH geometry. To test the viability of the present approach a series of deposition experiments was performed at constant potential on a rotating cylinder electrode with uniform current distribution. The rotation rate and the cathode geometry as well as the solutions used were the same as in the RCH experiments. Figure 10 shows a superposition of obtained results for the partial current densities of iron and nickel during single metal and alloy deposition. Since on a RCE each point represents a deposition experiment fewer points were taken. The data shown in Fig. 10 show a good correlation between the two different methods. They thus confirm that the conversion of a length scale into a potential scale based on numerical calculation of secondary current distribution gave correct results. In principle, one should also include mass transport effects (tertiary current distribution) in the calculation. However, the effect of transport on the total current distribution is relatively small under present conditions because the deposition of the major alloy component was kinetically controlled.

Compared to conventional experiments the use of the RCH cell in combination with small spot XRF analysis yields much more information. Nevertheless, certain limitations must be kept in mind. Since on the cathode of a RCH cell the deposit thickness varies with the local current density, the average current density and the deposition time must be chosen such that on one hand at the low current density end of the cathode enough deposit is formed to allow XRF analysis and on the other hand at the high current density end the current density and deposition time should be low enough to avoid dendrite formation and development of roughness which could reduce the accuracy of the XRF analysis. In the present experiments a constant deposition time of 10 min was used and the deposit thickness varied typically from 1 to 15 μm over the length of the cylindrical cathode, a range suitable for XRF analysis. Nevertheless, the analytical data at both ends of the cathode are less accurate than in the middle region, as is evidenced by the larger data scattering. The accuracy of the partial current density of the side reaction, obtained from the

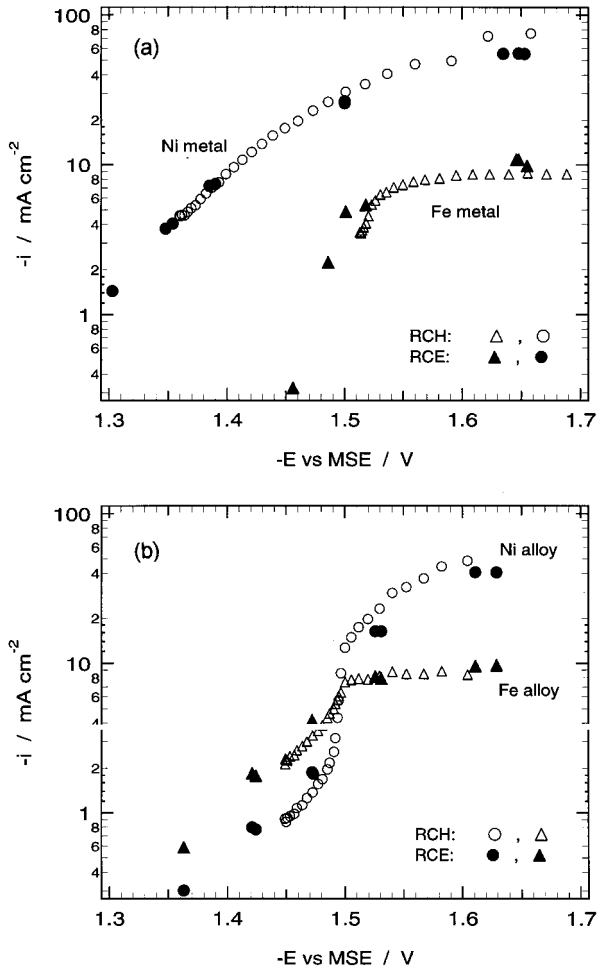

Fig. 10. Partial current densities of Ni and Fe determined from RCH cell and RCE experiments during single metal deposition (a) and during alloy deposition (b). Electrolyte concentration for single metal deposition: 0.025 M Fe and 0.2 M Ni, respectively. Electrolyte concentration for alloy deposition: 0.025 M Fe + 0.2 M Ni. Rotation rate: 800 rpm.

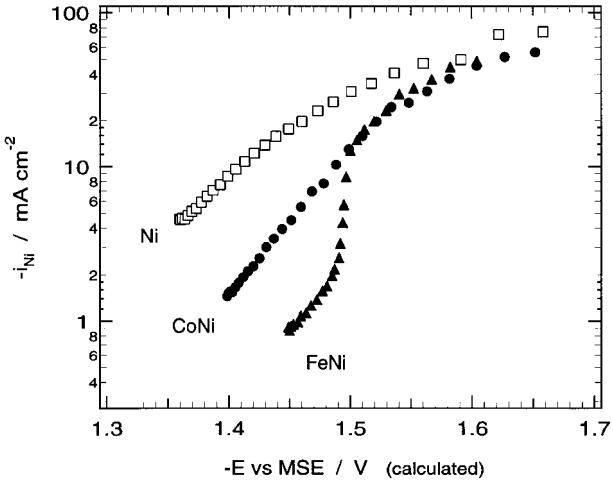

Fig. 11. Comparison of Ni partial current densities for single metal and for FeNi and CoNi alloy deposition in the RCH cell showing inhibition effect. Electrolyte concentrations: 0.2 M Ni, 0.025 M Fe + 0.2 M Ni, 0.025 M Co + 0.2 M Ni. Rotation rate: 800 rpm.

difference of the overall current density and the metal partial current densities, depends, not only on the accuracy of the XRF analysis, but also on that of the measured polarization curve on the RCE. It is well known unless a true steady state is reached at all potentials the obtained result of electrochemical polarization measurements will depend on scan rate. The scan rate of $2\,mV\,s^{-1}$ used in the present study may be considered sufficiently low for steady state conditions, but it is still fast compared to the experimental time of 10 min used in the deposition experiments. For the above-mentioned reasons, the results for the partial current density of the side reaction are expected to be somewhat less reliable than those for the partial current densities of metal deposition.

4.2. *Inhibiting and enhancing effects in anomalous codeposition*

In Fig. 11 the partial current density of Ni measured during single metal deposition is compared to that observed during codeposition with Co and Fe, respectively. Both codepositing metals lower the partial current density of nickel, meaning that they act as inhibitors for nickel deposition. The effect is more pronounced for iron than for cobalt. This observation is consistent with literature findings [30]. For both alloys, the inhibition effect on nickel disappears when the less noble species reaches its limiting current. This can be explained on the basis of literature models [14, 20] which state that inhibition is due to partial surface blocking by an adsorbed reaction intermediate of the less noble species. The surface coverage of the blocking species depends on the electrolyte concentration of the reacting ions in the immediate vicinity of the surface. As the limiting current of the less noble species is approached the concentration near the surface diminishes and so does the fractional coverage by the adsorbed intermediate. The data of Fig. 11 are consistent with this idea. In Fig. 3(a) the nickel partial current density exhibits a marked increase which coincides with the limiting current of iron shown in Fig. 3(b). A similar effect has been observed previously in the literature [17]. Interestingly, a similar abrupt kinetic transition has been observed in single metal iron deposition [31] and the sudden iron partial current density jump was related to the transition of the side reaction from a kinetic to mass transport control. In the present study the limiting current of the side reaction is reached before that of iron as evidenced by the data of Fig. 3(c). The observed transition in the nickel partial current density therefore is clearly due to iron not the side reaction. On the other hand, Fig. 6(a) shows no sharp transition in the nickel partial current density when the codepositing cobalt reaches the limiting current. The effect is being studied in our laboratory using numerical modeling and results will be reported in a later publication [32].

In Fig. 12 the iron partial current densities measured during single metal deposition and during codeposition with nickel and cobalt are presented. The ferrous ion concentration in the electrolyte as

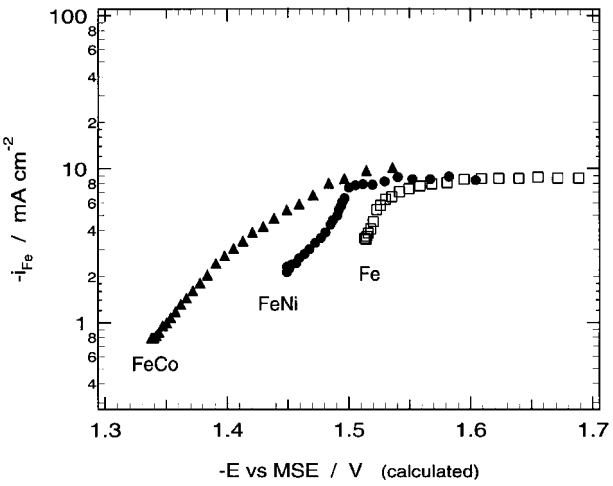

Fig. 12. Comparison of Fe partial current densities for single metal deposition and for FeNi and FeCo alloy deposition in the RCH cell. Electrolyte concentrations: 0.025 M Fe, 0.025 M Fe + 0.2 M Ni, 0.025 M Fe + 0.2 M Co. Rotation rate: 800 rpm.

well as the other conditions were kept the same in all experiments. The absence of nickel or cobalt sulfate, respectively, during single metal deposition was compensated by adding sodium sulfate (Table 1). The data of Fig. 12 show that the iron partial current density is enhanced by codepositing nickel or cobalt. The effect is more pronounced with cobalt than with nickel. It may be noted that within the accuracy of such measurements the limiting current plateau of iron is not significantly affected. This indicates that morphological effects such as, for example, an increase in real surface area cannot explain the observed enhancement of the partial current density of iron during alloy deposition, since they would also influence the limiting current. It is concluded that the codeposition of nickel and cobalt promotes the deposition of iron by changing the rate of the partial electrode reaction. Catalytic effects in codeposition have been described before [13] and quantitative modeling of such effects has been achieved for induced codeposition of molybdenum with nickel [29]. A slight increase in the deposition rate of iron from the alloy electrolyte compared to single metal deposition is suggested by certain data in the classical paper of Dahms and Croll [1] and in the study by Sasaki and Talbot [33]. The results of the present study clearly demonstrate the existence of an enhancing effect of cobalt and nickel on the deposition rate of iron during anomalous codeposition. The similarity of this effect with the behavior previously observed in induced codeposition of molybdenum with nickel suggests that a common description could be found covering anomalous, as well as induced, codeposition [34]. The problem is being further pursued in our laboratory using mathematical modelling [32]. Very recently Sasaki and Talbot [35] independently of the present work, found also an enhancing effect of nickel and cobalt on iron deposition.

5. Conclusion

The present study demonstrates that the RCH cell is a useful tool for the investigation of alloy deposition behaviour. It is particularly well suited for the elucidation of how the partial current densities of the reacting species vary with potential for different mass transport conditions and electrolyte compositions. Obtained results for anomalous codeposition of iron group metals Ni, Co, Fe confirmed that in the potential range where the deposition reactions are under kinetic control the less noble metal inhibits deposition of the more noble metal. For the inhibition of nickel the order is Fe > Co. The inhibiting effect disappears at the limiting current of the less noble metal. The present study provides strong evidence that in anomalous codeposition of iron group metals the reaction rate of the less noble metal is catalysed by the more noble component, the enhancing effect on iron deposition following the order Co > Ni.

Acknowledgements

The authors gratefully acknowledge the valued help from C. Madore for the calculation of the potential distribution in the RCH cell. This work was supported by Fonds National Suisse de la Recherche Scientifique, Bern.

References

[1] H. Dahms and I. M. Croll, *J. Electrochem. Soc.* **112** (1965) 771.
[2] P. C. Andricacos and L. T. Romankiw, 'Magnetically Soft Materials in Data Storage: Their Properties and Electrochemistry', *in Advances in Electrochemical Science and Engineering*, Vol. 3 (1994), p. 226.
[3] K. Ohashi, M. Ito and M. Watanabe, 'Application of Electroplating to Thin Film Heads: An Overview', *Electrochem. Soc. Proc.* **88-23** (1988) 525–42.
[4] P. L. Cavallotti, B. Bozzini, L. Nobili and G. Zangari, *J. Electrochim. Acta* **39** (1994) 1123.
[5] C. A. Ross, *Ann. Rev. Mater. Sci.* **24** (1994) 159.
[6] R. Chesnutt, *J. Appl.Physics.* **73** (1993) 6223.
[7] R. L. White, *Plat. Surf. Finish.* **75** (1988) 70.
[8] S. S. Djokic, M. D. Maksimovic and D. C. Stefanovic, *J. Appl. Electrochem.* **19** (1989) 802.
[9] P. Duke, T. Montelbano and L. Misel, *Plat. Surf. Finish.* **69** (1982) 61.
[10] B. Löchel, and A.Maciossek, *J. Electrochem. Soc.* **143** (1996) 3343.
[11] A. Thommes, W. Stark, K. Leyendecker, W. Bacher, H. Liebscher, and Ch. Jakob, 'LIGA Microstructures from a NiFe-Alloy: Preparation by Electroforming and their Magnetic Properties', *Electrochem. Soc. Proc.* **94-6** (1994) 89–102.
[12] A. Brenner, 'Electrodeposition of Alloys', Vols. 1–2 (Academic Press, New York, 1963).
[13] D. Landolt, *Electrochim. Acta* **39** (1994) 1075.
[14] M. Matlosz, *J. Electrochem. Soc.* **140** (1993) 2272.
[15] D. Gangasingh and J. B. Talbot, *J. Electrochem. Soc.* **138** (1991) 3605.
[16] W. Grande and J. B. Talbot, *J. Electrochem. Soc.* **140** (1993) 675.
[17] P. C. Andricacos, C. Arana, J. Tabib, J. Dukovic and L. T. Romankiw, *J. Electrochem. Soc.* **136** (1989) 1336.
[18] K. H. Wong, P. C. Andricacos and L. T. Romankiw, 'Effect of Fe(II) Concentration on the Electrodeposition of Nickel-Iron Alloys', *Electrochem. Soc. Proc.* **90-8** (1990) 387–396.

[19] S. Hessami and C. W. Tobias, *J. Electrochem. Soc.* **136** (1989) 3611.
[20] B. C. Baker and A. C. West, *ibid.* **144** (1997) 169.
[21] C. Madore and D. Landolt, *Plat. Surf. Finish* **80** (1993) 73.
[22] C. Madore, A. C. West, M. Matlosz and D. Landolt, *Electrochim. Acta* **37** (1991) 69.
[23] C. Madore, PhD thesis no. 1189, Ecole Polytechnique Fédéral Lausanne, Switzerland (1993).
[24] C. Madore, M. Matlosz, D. Landolt, *J. Appl. Electrochem.* **22** (1992) 1155.
[25] C. Madore, D. Landolt, C. Hassenpflug, J. A. Hermann, *Plat. Surf. Finish.* **82** (1995) 36.
[26] A. C. West, M. Matlosz and D. Landolt, *J. Appl. Electrochem.* **22** (1992) 301.
[27] M. Matlosz, C. Creton, C. Clerc and D. Landolt, *J. Electrochem. Soc.* **134** (1987) 3015.
[28] M. Matlosz, 'Boundary Element Calculations in Design', *Electrochem. Soc. Proc.* **95-11** (1995) 221–36.
[29] E. J. Podlaha and D. Landolt, *J. Electrochem. Soc.* **143** (1996) 885.
[30] P. C. Andricacos, 'On the Anomalous Codeposition of Ferrous Metal Alloys', *Electrochem. Soc. Proc.* **94-31** (1994) 157–76.
[31] A. A. El Miligy, F. Hilbert and W. J. Lorenz, *J. Electrochem. Soc.* **120** (1973) 247.
[32] N. Zech, E. J. Podlaha and D. Landolt, to be published.
[33] K. Y. Sasaki and J. B. Talbot, *J. Electrochem. Soc.* **142** (1995) 775.
[34] D. Landolt, N. Zech, E. J. Podlaha, *Z. Phys. Chem.*, submitted.
[35] K. Y. Sasaki and J. B. Talbot, *J. Electrochem. Soc.* **145** (1998) 981.